NANO LETTERS

pubs.acs.org/NanoLett

Epitaxial Heterostructures of Ultrathin Topological Insulator Nanoplate and Graphene

Wenhui Dang,† Hailin Peng,† Hui Li, Pu Wang, and Zhongfan Liu*

Center for Nanochemistry, Beijing National Laboratory for Molecular Sciences (BNLMS), State Key Laboratory for Structural Chemistry of Unstable and Stable Species, College of Chemistry and Molecular Engineering, Peking University, Beijing 100871, People's Republic of China

ABSTRACT The authors present a van der Waals epitaxy of high-quality ultrathin nanoplates of topological insulator Bi_2Se_3 on a pristine graphene substrate using a simple vapor-phase deposition method. Sub-10-nm-thick nanoplates of layered Bi_2Se_3 with defined orientations can be epitaxially grown on a few-layer pristine graphene substrate. We show the evolution of Raman spectra with the number of Bi_2Se_3 layers on few-layer graphene. Bi_2Se_3 nanoplates with a thickness of three quintuple-layers (3-QL) exhibit the strongest Raman intensity. Strain effects in the Bi_2Se_3/graphene nanoplate heterostructures is also studied by Raman spectroscopy. 1-QL and 2-QL Bi_2Se_3 nanoplates experience tensile stress, consistent with compressive stress in single-layer and bilayer graphene substrates. Our results suggest an approach for the synthesis of epitaxial heterostructures that consist of an ultrathin topological insulator and graphene, which may be a new direction for electronic and spintronic applications.

KEYWORDS Topological insulator, graphene, Dirac materials, bismuth selenide, van der Waals epitaxy

Dirac materials, such as graphene and topological insulators, have received extensive attention only in the past few years because of their distinctive band structures and physical properties.[1−4] The electrons in Dirac materials display a linear energy-momentum "relativistic" dispersion accurately described by the massless Dirac Hamiltonian.[5] Three-dimensional (3D) topological insulators were recently recognized as new state of quantum matter with an insulating bulk state and current-carrying massless Dirac surface states.[6−8] Unlike graphene with even numbers of spin-degenerate Dirac cones, most 3D topological insulators exhibit an odd number of topologically spin-polarized Dirac cones on their surfaces.[9−15] Bismuth selenide (Bi_2Se_3), a typical thermoelectric and infrared detector material,[16] serves as a reference topological insulator material with a large nontrivial bulk gap of ∼0.3 eV (equivalent to 3600 K) and a simple single-Dirac-cone surface state at the Γ point.[9,10]

Nanostructured Dirac materials, such as two-dimensional (2D) ultrathin films and nanoribbons with extremely large surface-to-volume ratios and/or distinct edge effects, attract much interest as possible materials for the next generation of electronic and spintronic devices.[15,17−20] Compared to bulk materials, nanostructured topological insulators are advantageous, because they suppress the residual conductance in the bulk originating from unintentional and uncontrolled doping states. Nanoribbons of topological insulator materials were synthesized by a vapor−liquid−solid (VLS) process.[20,21] Recent transport measurements of Bi_2Se_3 nanoribbons exhibited pronounced Aharonov−Bohm oscillations associated with the topological surface states.[20] More recently, the Kondo effect was observed at temperatures below ∼30 K in Bi_2Se_3 nanoribbons with magnetic doping.[22] Ultrathin film forms of Bi_2Se_3 and Bi_2Te_3 were obtained by molecular beam epitaxy (MBE) growth.[23,24] The Landau quantization of the topological surface states in the Bi_2Se_3 MBE film was recently observed in magnetic field by using scanning tunneling microscopy and spectroscopy (STM/STS).[25] In addition, mechanical exfoliation of thin sheets from bulk crystals has achieved good quality Bi_2Te_3 films, but with irregular shapes and low yield.[26,27] To date, the precisely controlled growth of nanostructured topological insulators with defined sizes and orientations is desirable, because the finite-size effects and integration of nanoscale building blocks are important for actual devices.[28,29]

Heterostructures involving these intriguing Dirac materials, such as graphene p−n junctions,[1,30] and topological insulator−superconductor junctions,[4,31] present an exciting new direction in theoretical and experimental research. Interlayer interactions of Dirac fermions make nanoscale Bi_2Se_3/graphene heterostructures very appealing for future electronic and spintronic applications. However, it remains highly desirable to synthesize high-quality heterostructures of Dirac materials. Chemical decorations of various inorganic nanoparticles on graphene oxide sheets with various degrees of oxidation have been reported recently.[32−37] In contrast, due to the chemical inertness and low binding energies for

* To whom correspondence should be addressed, zfliu@pku.edu.cn.

† These authors contributed equally to this work.

Received for review: 03/17/2010
Published on Web: 07/12/2010

DOI: 10.1021/nl100938e | *Nano Lett.* **2010,** *10,* 2870–2876

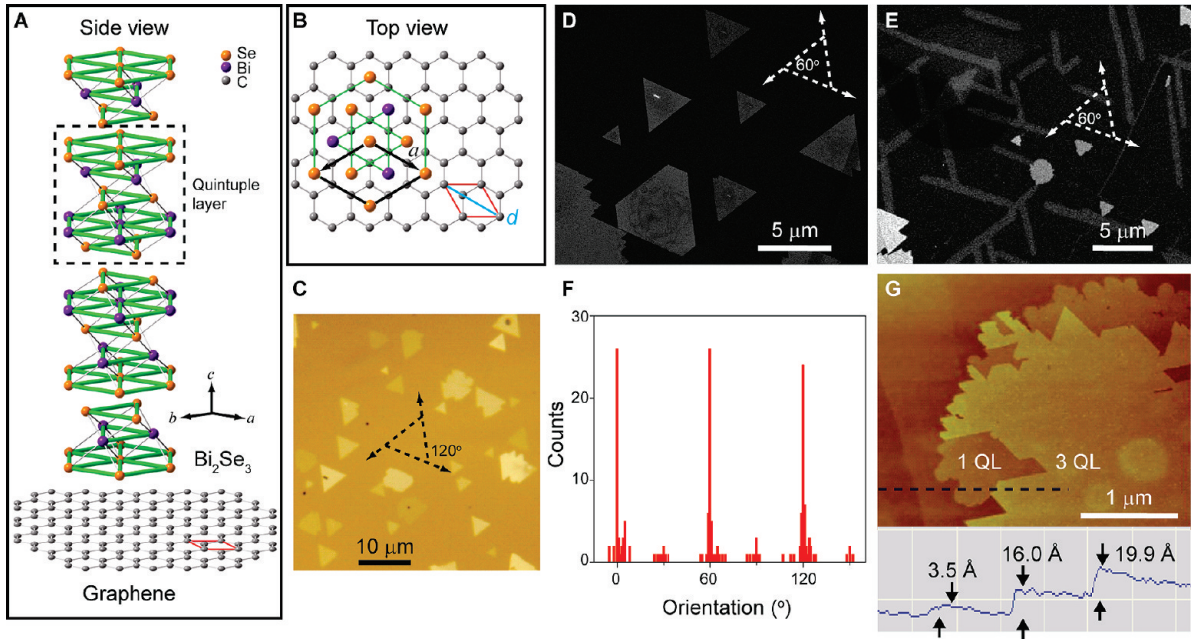

FIGURE 1. Vapor-phase synthesis of Bi_2Se_3 nanoplates on few-layer graphene substrates via van der Waals epitaxy. (A, B) Schematic for epitaxial growth mode. (C) A typical photograph of Bi_2Se_3 nanoplates epitaxially grown on a multilayer graphene substrate. (D) SEM image of triangular or hexagonal nanoplates with the same orientation. (E) SEM image of ultrathin nanoribbons aligned in three orientations at 120° to one another (indicated by a triangle and arrows). (F) Histogram of orientation distribution of triangular/hexagonal nanoplates. (G) AFM image of a three quintuple-layer (QL) Bi_2Se_3 nanoplate on a multilayer graphene substrate.

adsorbates, the decoration method of functional nanocrystals on the pristine graphene is lacking. Here we present a simple vapor-phase deposition of high-quality ultrathin nanoplates of Bi_2Se_3 with defined orientations and controlled thicknesses (1-QL to 10-QL) on a few-layer pristine graphene substrate by van der Waals epitaxy. The van der Waals interactions, present in both few-layer graphene and the Bi_2Se_3 crystal structure, allowed us to assemble the nanoplates of graphene and Bi_2Se_3 into a heterostructure. The single crystalline Bi_2Se_3 nanoplates are continuous and uniform with atomically smooth surfaces. We carried out optical microscopy, scanning electron microscopy (SEM), transmission electron microscopy (TEM), atomic force microscopy (AFM), and micro-Raman spectroscopy to demonstrate the unusual structure and properties of such quasi-2D Dirac material heterostructures. We show an evolution of Raman spectra with the number of Bi_2Se_3 layers on few-layer graphene. Strain effect in the Bi_2Se_3/graphene nanoplate heterostructures is revealed by micro-Raman spectroscopy. The van der Waals epitaxy can lead to a new technology for producing heterostructures of pristine graphene and 2D layered materials with van der Waals gaps, paving the way for nanoelectronics, thermoelectrics, and other possible practical applications.

Layered Bi_2Se_3 has a rhombohedral crystal structure in the space group D^5_{3d} ($R\bar{3}m$) (Figure 1A).[38] Each quintuple layer (QL) in Bi_2Se_3 is ordered in a Se−Bi−Se−Bi−Se sequence along the c axis and form planar, covalently bonded sheets linked together predominantly via van der Waals interactions. The unit cell (lattice constants $a \sim 4.140$ Å, $c \sim 28.636$ Å) spans over three QLs. The thickness of each QL is ~9.55 Å. Graphene, a single layer of sp^2-bonded carbon atoms with a honeycomb lattice structure, exhibits a hexagonal symmetry with the lattice constant $a = 2.46$ Å. The length of the C−C bond in graphene is ~1.42 Å. The hexagonal periodicity of the graphene surface along which the Bi_2Se_3 aligns is $d = 4.26$ Å, which has a lattice mismatch of ~2.9% with Bi_2Se_3 (Figure 1B). However, the use of the van der Waals interface efficiently relaxes the lattice-matching condition usually encountered in heteroepitaxial growth of layered materials.[39−41]

Different from the metal-catalyzed VLS growth of nanoribbons of Bi_2Se_3 and other chalcogenides reported recently,[21,42−45] Bi_2Se_3 nanoplates were grown on few-layer graphene substrates using a catalyst-free vapor transport and deposition method inside a 12 in. horizontal tube furnace equipped with a 1 in. diameter quartz tube. Few-layer graphene flakes were previously prepared by micromechanical cleavage of Kish graphite (Covalent Materials Corp.) on top of an oxidized silicon substrate (300 nm thick SiO_2). Bi_2Se_3 powder was placed into the hot center region of the tube furnace (460−500 °C) as the precursors for evaporation. Ultrapure argon acted as a carrier gas to transport the vapor downstream. The SiO_2/Si substrates decorated with few-layer graphene were placed downstream at certain positions to accurately set the deposition temperature. The tube was initially pumped to a base pressure of 10 mTorr and flushed with the carrier gas repeatedly to remove oxygen contamination. Typical synthesis conditions are pressure 100 Torr, growth time 5−30 min, and gas flow

DOI: 10.1021/nl100938e | *Nano Lett.* **2010,** *10,* 2870–2876

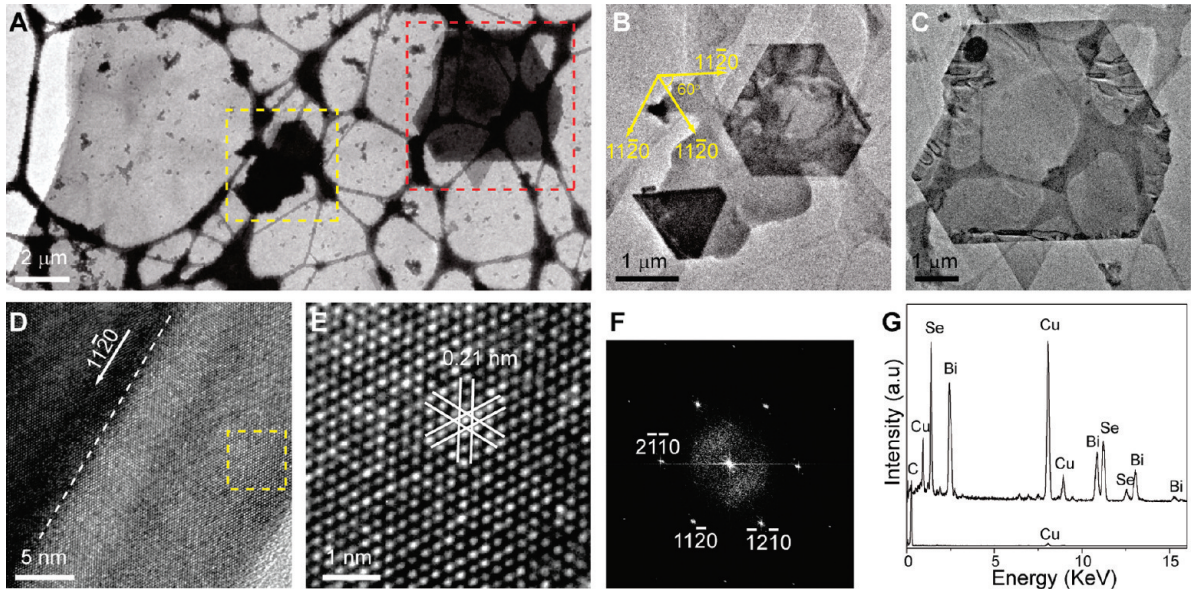

FIGURE 2. (A) TEM images of epitaxial heterostructure of ultrathin Bi_2Se_3 nanoplate and few-layer graphene. (B, C) Magnified TEM images of the yellow and red squares in (A), respectively. The nanoplates have the same orientation to one another. (D) HRTEM image of Bi_2Se_3 nanoplate with a step at the edge. The step edge of the nanoplate is highlighted with a white dashed line to show the orientation along the [11−20]. (E, F) HRTEM image of the yellow square in (D) and corresponding fast Fourier transformation (FFT) pattern. (G) EDX analysis of the Bi_2Se_3 nanoplate (up) and few-layer graphene substrate (bottom). The Cu signal comes from the Cu grid.

50−100 sccm (standard cubic centimeters per minute). The substrate temperature is important for controlling the morphology and thicknesses of the products (Figure S1, Supporting Information). Continuous, ultrathin Bi_2Se_3 nanoplates preferentially grew on graphene in the 330−380 °C zone while fractional, thick Bi_2Se_3 nanoplates preferred to deposit at the edges or defect sites of graphene in the colder zone (below ∼300 °C). The Bi_2Se_3/graphene nanoplate heterostructures were characterized using an Olympus DX51 optical microscope, Hitachi S-4800 SEM, AFM (Nanoscope IIIA, Digital Instruments), FEI Tecnai F30 TEM equipped with an energy dispersive X-ray spectrometer (EDX), and micro-Raman spectroscopy.

The as-grown Bi_2Se_3/graphene heterostructures were first identified by their optical contrast in the optical microscope. Figure 1C shows a typical photograph of Bi_2Se_3 nanoplates grown on a multilayer graphene substrate. The Bi_2Se_3 nanoplates have triangular or hexagonal shapes with lateral dimensions of several hundred nanometers to several micrometers. Individual nanoplates show uniform color contrast, indicating a uniform thickness along the entire plane of the nanoplate. Remarkably, all the triangular nanoplates have the same orientation, suggesting the epitaxy of Bi_2Se_3 on graphene layer. From the SEM image, the Bi_2Se_3 nanoplates with uniform thicknesses were aligned in the same orientation on the graphene layer (Figure 1D). Here the orientations of the nanoplates' edges occur at multiples of 60°, consistent with the two-dimensional triangular lattice of the Bi_2Se_3 quintuple layer. Some ultrathin Bi_2Se_3 nanoribbons aligned in three major orientations at 120° to one another were also observed on the graphene layer (Figure 1E). Figure 1F illustrates the orientation distribution of epitaxial triangular nanoplates. The edges of these nanoplates are mostly along the direction of 0°, 60°, and 120°. Some Bi_2Se_3 nanoplates deviate from these major directions, probably due to the weak van der Waals interaction, lattice mismatch, and perturbations of step, corrugation, or defect on multilayer graphene substrates. Figure 1G shows a typical AFM image of an ultrathin Bi_2Se_3 nanoplate with 3-QL thickness grown on a few-layer graphene substrate. The terrace structures of both Bi_2Se_3 and graphene layer were observed. A line-cut across these terraces revealed the step height of few-layer graphene and the first layer of Bi_2Se_3 sheet are about 0.35 Å and 16.0 Å, respectively (Figure S2, Supporting Information). Another step of the Bi_2Se_3 sheet has the height of 19.9 Å, consistent with the 2-QL thickness of Bi_2Se_3. Extensive AFM analyses of the terraced Bi_2Se_3 nanoplates show the average step height is 9.8 Å (Figure S3, Supporting Information). Note that Bi_2Se_3 nanoplates with thickness of ≥3-QL usually have smooth side walls and defined orientations, whereas single-QL nanoplates exhibit rough edges.

In order to further study the structure and chemical composition of the epitaxial heterostructures, we characterized Bi_2Se_3/graphene nanoplate heterostructures using TEM and EDX. Few-layer graphene sheets decorated with Bi_2Se_3 nanoplates were mechanically transferred from the SiO_2/Si substrate to a lacey carbon support film on a TEM copper grid with the assistance of a drop of dilute HF solution (2 % v/v). Figure 2A shows a typical TEM image of the Bi_2Se_3/graphene nanoplate heterostructure. From the close-up views, hexagonal and triangular nanoplates aligned in the

DOI: 10.1021/nl100938e | *Nano Lett.* **2010,** *10,* 2870–2876

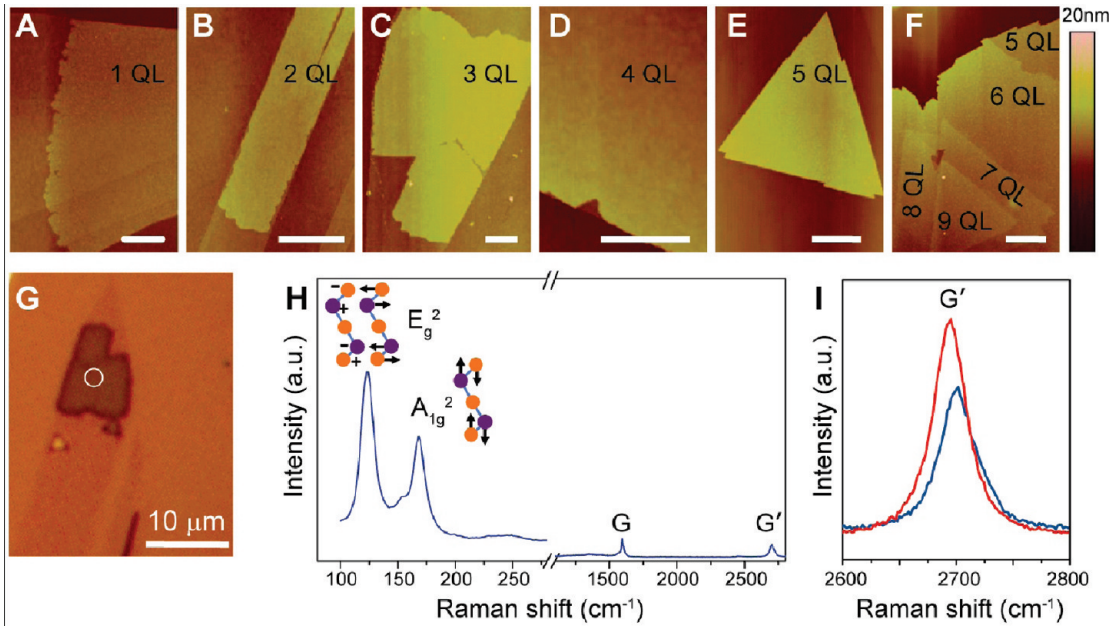

FIGURE 3. Epitaxial growth of large-area, ultrathin Bi_2Se_3 nanoplate with different thickness on few-layer graphene. (A−F) AFM images of ultrathin Bi_2Se_3 nanoplates with different thicknesses grown on few-layer graphene: (A) 1-QL Bi_2Se_3 nanoplate on bilayer graphene; (B) 2-QL Bi_2Se_3 nanoplate on bilayer graphene; (C) 3-QL Bi_2Se_3 nanoplate on single-layer graphene; (D) 4-QL Bi_2Se_3 nanoplate on three-layer graphene; (E) 5-QL Bi_2Se_3 nanoplate on few-layer graphene; (F) Layered Bi_2Se_3 nanoplates (5−9-QL) on few-layer graphene. Scale bars in (A−F) are 1 μm. (G) Optical image of a 3-QL Bi_2Se_3 nanoplate on single-layer graphene. (H) Raman spectra of 3-QL Bi_2Se_3 nanoplate grown on single-layer graphene using green (514 nm) laser excitation. The recorded position was indicated by the white circle in (G). (I) Close-up view of G′ peaks of the same single-layer graphene substrate with (blue) and without (red) the decoration of the Bi_2Se_3 nanoplate, respectively.

same orientation are clearly visible (Figure 2, panels B and C). The lateral dimension of nanoplate can reach several micrometers.

Interestingly, the few-layer graphene membrane with atomic thickness and low atomic mass provides an excellent support for high-resolution TEM (HRTEM) imaging. Note that the Bi_2Se_3 nanoplate is much more stable than the few-layer graphene during the HRTEM imaging operated with an accelerating voltage of 300 keV. A HRTEM image shows a Bi_2Se_3 nanoplate with a clear thickness contrast (Figure 2D), consistent with the terraced structure nature of layered Bi_2Se_3 nanoplates. An enlarged TEM image (Figure 2E) shows hexagonal lattice fringes, with a lattice spacing of 0.21 nm, agreeing well with the spacing of the (11−20) planes of layered Bi_2Se_3. The corresponding FFT pattern exhibits a clear hexagonally symmetric spot pattern, confirming the single crystalline nature. Similar to the Bi_2Se_3 nanoribbons,[20,21] the nanoplates grow along the [11−20] direction, with (01−10) facets as side surfaces and (0001) facets as top and bottom surfaces. EDX analyses reveal uniform chemical composition of the nanoplates with a Bi:Se atomic ratio of 2:3, indicating stoichiometric Bi_2Se_3 free of detectable impurities within the experimental uncertainty limit of EDX analyses (<2%) (Figure 2G). Moiré-type modulation structures were observed in some Bi_2Se_3/graphene nanoplate heterostructures, originating from the interactions between closely placed layers of two materials with different lattice constants and/or orientations (data not shown).

Large-area, continuous, ultrathin Bi_2Se_3 nanoplates with various thicknesses (1QL to 9QL) can epitaxially grow on few-layer graphene substrates, indicated by our AFM measurements (Figure 3A−F). Even from the very initial stage of epitaxial growth, a smooth and uniform Bi_2Se_3 film grows epitaxially on a graphene substrate. Note that the growth of continuous, atomic flat Bi_2Se_3 films can grow over the steps on graphene and terminate at the edges of graphene.

Raman spectroscopy is a powerful tool for the study and characterization of both layered Bi_2Se_3 and graphene, respectively.[46−48] Few-layer graphene substrates were identified with the optical microscope and subsequently confirmed by Raman spectroscopy and AFM measurements. Figure 3G shows a typical optical image of a 3-QL nanoplate of Bi_2Se_3 on single-layer graphene. The Raman measurements are performed at room temperature with a Renishaw spectrometer with notch filters cutting at ~100 cm^{-1}. The excitation spot size is about 1 μm. All Raman spectra are recorded at very low power levels $P < 0.2$ mW and $P < 0.7$ mW on the sample surface for 514 and 633 nm excitation lasers, respectively. Sample damage is avoided under such measurement conditions, which is confirmed by AFM measurements. Figure 3H shows a typical Raman spectrum ranging from 100 to 2800 cm^{-1} at 514 nm laser excitation for the 3-QL nanoplate of Bi_2Se_3 on a single-layer graphene. At the low frequency region, two characteristic peaks of rhombohedral Bi_2Se_3 at 131 and 174 cm^{-1} correspond to an in-plane vibrational mode (E_g^2) and an out-of-plane

DOI: 10.1021/nl100938e | *Nano Lett.* **2010,** *10,* 2870–2876

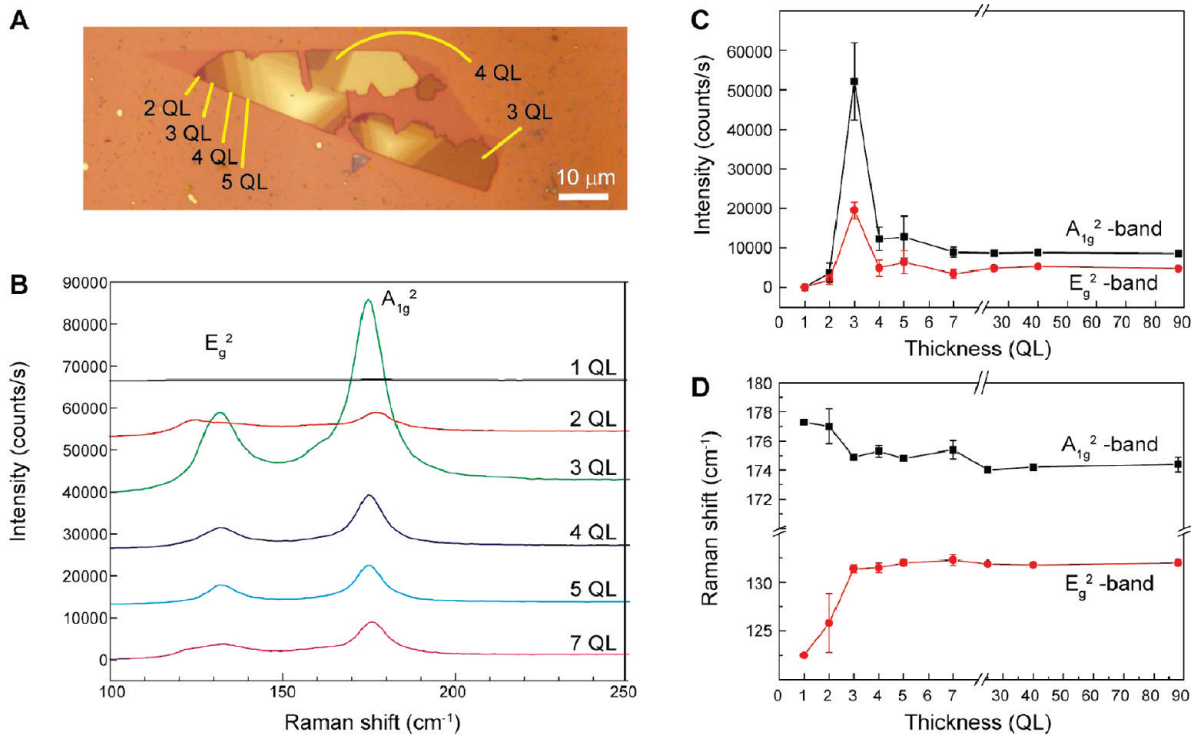

FIGURE 4. (A) Optical image of layered Bi_2Se_3 nanoplates with obvious contrast grown on a few-layer graphene substrate. (B) Evolution of the Raman spectra at 633 nm laser with the number of Bi_2Se_3 quintuple layers (QLs). (C) Intensity variation of A_{1g}^2 and E_g^2 bands for Bi_2Se_3 nanoplates as a function of thickness. The 3-QL films have the strongest Raman signals. (D) Evolution of the Raman frequency position with the number of layers. A_{1g}^2 band upshift $\Delta\omega = 3.3$ cm^{-1}; E_g^2 band downshift $\Delta\omega = 9.2$ cm^{-1}.

vibrational mode (A_{1g}^2) of Se−Bi−Se−Bi−Se lattice vibration, respectively.[46] Note that there is no significant change in the shapes of the characteristic E_g^2 and A_{1g}^2 peaks of Bi_2Se_3 nanoplates compared with that of the bulk crystal (Figures S4 and S5, Supporting Information), consistent with the good crystallization nature of ultrathin Bi_2Se_3 films. At the high frequency region, the two characteristic peaks for graphene at ~1580 (G-band) and ~2700 cm^{-1} (G′-band) are shown, assigned to the stretching of the C−C bond and a second-order two-phonon process in sp^2 carbon systems, respectively.[48] For clarity, Figure 3I shows the G′ peaks of the same single-layer graphene with and without the decoration of Bi_2Se_3 nanoplates, respectively. The G′ peak of the pristine graphene was well fitted by a sharp and symmetric Lorentzian peak, consistent with the feature of single-layer graphene.[47] The single-layer graphene covered with 3-QL Bi_2Se_3 nanoplate has a broader and up-shifted G′ band, which may be closely related to the interaction of graphene and the surface state of Bi_2Se_3.

We have carried out detailed micro-Raman scattering from Bi_2Se_3 ultrathin nanoplates with different layers at room temperature in the backscattering geometry. Remarkably, layer number of Bi_2Se_3 films on few-layer graphene substrates can be roughly identified through the optical color contrast (Figure 4A). Figure 4B plots the evolution of Raman spectra for a 633 nm excitation as a function of the number of Bi_2Se_3 layers. Two characteristic E_g^2 and A_{1g}^2 vibrational modes at ~131 and ~174 cm^{-1} were detected as expected.[41] The Raman intensity and frequency shift variation with thickness (QLs) are obvious. Our extensive Raman measurements show that 3-QL thick Bi_2Se_3 nanoplates have the strongest Raman intensity (Figure 4C). An enhancement factor may exist for Raman scattering of 3-QL Bi_2Se_3 nanoplates and needs to be further addressed. We noted similar work by Shahil and colleagues on Raman spectra of mechanically exfoliated Bi_2Te_3 quintuples during the review process of our work.[49] In Bi_2Te_3 quintuples with thickness ranging from bulk limit to ~4 nm, the intensity of the out-of-plane vibrations increases with decreasing thickness, consistent with the results of Bi_2Se_3 nanoplates.

Figure 4D plots the evolution of the Raman frequency position for Bi_2Se_3 nanoplates as a function of the thickness. Compared to the Raman peak positions of multilayer (≥3-QL) Bi_2Se_3 nanoplates, the single-QL and 2-QL films displayed a significant downshift (~9.2 cm^{-1}) of in-plane vibrational mode with E_g^2 symmetry, while a upward shift (~3.3 cm^{-1}) of out-of-plane vibration mode with A_{1g}^2 symmetry was observed. These results indicate that Bi_2Se_3 nanoplates with a thickness of ≤2-QL is under significant stress.[50,51] Such stress is always introduced into epitaxial layers due to the lattice mismatch between crystal and substrate (here ~2.9%).[52−54] Because the hexagonal periodicity of the graphene surface is slightly larger than that of the Bi_2Se_3 crystal lattice, Bi_2Se_3 epitaxial nanoplate (below 2-QL) experiences tensile stress, which is parallel to the film plane.[53] This result is consistent with the downward shift of

DOI: 10.1021/nl100938e | *Nano Lett.* **2010,** *10,* 2870–2876

the in-plane vibrational mode. The upward shift of the out-of-plane vibrational mode strongly suggests that compressive stress exists in the *c* axis direction.[55] Our measurements demonstrate that there is no obvious shift of Raman position when the thickness is above 3-QL, indicating that the stress inside the Bi_2Se_3 epitaxial layer with thickness of ≥3-QL disappears.[50,54]

The tensile stress of Bi_2Se_3 nanoplates might give rise to a compressive stress in the few-layer graphene substrate. Indeed, we observed an obvious upward shift of the G-band for single-layer and bilayer graphene covered by 1-QL or 2-QL Bi_2Se_3 nanoplates (Figure S6, Supporting Information). The upward shift of G-band ranges from 5 to 10 cm^{-1}, indicating significant compressive stress in the graphene substrate.[56−59]

In summary, van der Waals epitaxy of large area, high-quality, ultrathin topological insulator Bi_2Se_3 nanoplates on few-layer graphene has been achieved by a catalyst-free vapor transport and deposition method. The van der Waals epitaxy suggests an interesting approach for producing heterostructures involving pristine graphene and layered topological insulators. The detailed Raman measurements reveal the strain effects in the Bi_2Se_3/graphene nanoplate heterostructures and display an evolution of Raman spectra with a number of Bi_2Se_3 layers. The Bi_2Se_3/graphene nanoplate heterostructure provides a good candidate for the study of the unusual interaction of Dirac fermions, which may open new exciting opportunities in future electronic and spintronic devices.

Acknowledgment. H.P. would like to thank Desheng Kong, Stefan Meister, and Dr. Keji Lai for helpful discussions. This work was supported by NSFC (20973007, 20973013, 50821061) and MOST (2007CB936203).

Supporting Information Available. More AFM and Raman measurement data. This material is available free of charge via the Internet at http://pubs.acs.org.

REFERENCES AND NOTES

(1) Katsnelson, M. I.; Novoselov, K. S.; Geim, A. K. *Nat. Phys.* **2006**, *2*, 620.
(2) Geim, A. K.; Novoselov, K. S. *Nat. Mater.* **2007**, *6*, 183.
(3) Castro Neto, A. H.; Guinea, F.; Peres, N. M. R.; Novoselov, K. S.; Geim, A. K. *Rev. Mod. Phys.* **2009**, *81*, 109.
(4) Hasan, M. Z.; Kane, C. L. arXiv:1002.3895v1.
(5) Biswas, R. R.; Balatsky, A. V. arXiv: 0910.4604v2.
(6) Fu, L.; Kane, C. L.; Mele, E. J. *Phys. Rev. Lett.* **2007**, *98*, 106803.
(7) Moore, J. E.; Balents, L. *Phys. Rev. B* **2007**, *75*, 121306.
(8) Qi, X. L.; Hughes, T. L.; Zhang, S. C. *Phys. Rev. B* **2008**, *78*, 195424.
(9) Xia, Y.; Qian, D.; Hsieh, D.; Wray, L.; Pal, A.; Lin, H.; Bansil, A.; Grauer, D.; Hor, Y. S.; Cava, R. J.; Hasan, M. Z. *Nat. Phys.* **2009**, *5*, 398.
(10) Zhang, H.; Liu, C.-X.; Qi, X.-L.; Dai, X.; Fang, Z.; Zhang, S.-C. *Nat. Phys.* **2009**, *5*, 438.
(11) Chen, Y. L.; Analytis, J. G.; Chu, J. H.; Liu, Z. K.; Mo, S.-K.; Qi, X. L.; Zhang, H. J.; Lu, D. H.; Dai, X.; Fang, Z.; Zhang, S. C.; Fisher, I. R.; Hussain, Z.; Shen, Z.-X. *Science* **2009**, *325*, 178.
(12) Hsieh, D.; Xia, Y.; Qian, D.; Wray, L.; Dil, J. H.; Meier, F.; Osterwalder, J.; Patthey, L.; Checkelsky, J. G.; Ong, N. P.; Fedorov, A. V.; Lin, H.; Bansil, A.; Grauer, D.; Hor, Y. S.; Cava, R. J.; Hasan, M. Z. *Nature* **2009**, *460*, 1101.
(13) Hsieh, D.; Xia, Y.; Qian, D.; Wray, L.; Meier, F.; Dil, J. H.; Osterwalder, J.; Patthey, L.; Fedorov, A. V.; Lin, H.; Bansil, A.; Grauer, D.; Hor, Y. S.; Cava, R. J.; Hasan, M. Z. *Phys. Rev. Lett.* **2009**, *103*.
(14) Roushan, P.; Seo, J.; Parker, C. V.; Hor, Y. S.; Hsieh, D.; Qian, D.; Richardella, A.; Hasan, M. Z.; Cava, R. J.; Yazdani, A. *Nature* **2009**, *460*, 1106.
(15) Zhang, T.; Cheng, P.; Chen, X.; Jia, J. F.; Ma, X. C.; He, K.; Wang, L. L.; Zhang, H. J.; Dai, X.; Fang, Z.; Xie, X. C.; Xue, Q. K. *Phys. Rev. Lett.* **2009**, *103*.
(16) Mishra, S. K.; Satpathy, S.; Jepsen, O. *J. Phys.: Condens. Matter* **1997**, *9*, 461.
(17) Barone, V.; Hod, O.; Scuseria, G. E. *Nano Lett.* **2006**, *6*, 2748.
(18) Brey, L.; Fertig, H. A. *Phys. Rev. B* **2006**, *73*.
(19) Li, X. L.; Wang, X. R.; Zhang, L.; Lee, S. W.; Dai, H. J. *Science* **2008**, *319*, 1229.
(20) Peng, H. L.; Lai, K.; Kong, D.; Meister, S.; Chen, Y.; Qi, X.-L.; Zhang, S.-C.; Shen, Z.-X.; Cui, Y. *Nat. Mater.* **2010**, *9*, 225.
(21) Kong, D. S.; Randel, J. C.; Peng, H. L.; Cha, J. J.; Meister, S.; Lai, K. J.; Chen, Y. L.; Shen, Z. X.; Manoharan, H. C.; Cui, Y. *Nano Lett.* **2010**, *10*, 329.
(22) Cha, J. J.; Williams, J. R.; Kong, D.; Meister, S.; Peng, H.; Bestwick, A. J.; Gallagher, P.; Goldhaber-Gordon, D.; Cui, Y. *Nano Lett.* **2010**, *10*, 1076.
(23) Zhang, G.; Qin, H.; Teng, J.; Guo, J.; Guo, Q.; Dai, X.; Fang, Z.; Wu, K. *Appl. Phys. Lett.* **2009**, *95*, No. 053114.
(24) Zhang, T.; Cheng, P.; Chen, X.; Jia, J.-F.; Ma, X.; He, K.; Wang, L.; Zhang, H.; Dai, X.; Fang, Z.; Xie, X.; Xue, Q.-K. *Phys. Rev. Lett.* **2009**, *103*, 266803.
(25) Cheng, P.; Song, C.; Zhang, T.; Zhang, Y.; Wang, Y.; Jia, J.; Wang, J.; Zhu, B.; Chen, X.; Ma, X.; He, K.; Wang, L.; Dai, X.; Fang, Z.; Xie, X. C.; Qi, X.-L.; Liu, C.-X.; Zhang, S.-C.; Xue, Q.-K. arXiv: 1001.3220.
(26) Teweldebrhan, D.; Goyal, V.; Rahman, M.; Balandin, A. A. *Appl. Phys. Lett.* **2010**, *96*, No. 053107.
(27) Teweldebrhan, D.; Goyal, V.; Balandin, A. A. *Nano Lett.* **2010**, *10*, 1209.
(28) Linder, J.; Yokoyama, T.; Sudb, A. *Phys. Rev. B* **2009**, *80*, 205401.
(29) Liu, C.-X.; Zhang, H.; Yan, B.; Qi, X.-L.; Frauenheim, T.; Dai, X.; Fang, Z.; Zhang, S.-C. *Phys. Rev. B* **2010**, *81*, No. 041307.
(30) Beenakker, C. W. J. *Rev. Mod. Phys.* **2008**, *80*, 1337.
(31) Fu, L.; Kane, C. L. *Phys. Rev. Lett.* **2008**, *100*, No. 096407.
(32) Wang, X. R.; Tabakman, S. M.; Dai, H. J. *J. Am. Chem. Soc.* **2008**, *130*, 8152.
(33) Cao, A. N.; Liu, Z.; Chu, S. S.; Wu, M. H.; Ye, Z. M.; Cai, Z. W.; Chang, Y. L.; Wang, S. F.; Gong, Q. H.; Liu, Y. F. *Adv. Mater. 22*, 10.
(34) Nethravathi, C.; Nisha, T.; Ravishankar, N.; Shivakumara, C.; Rajamathi, M. *Carbon* **2009**, *47*, 2054.
(35) Kim, Y.-J.; Lee, J.-H.; Yi, G.-C. *Appl. Phys. Lett.* **2009**, *95*, 213101.
(36) Wang, H.; Robinson, J. T.; Diankov, G.; Dai, H. *J. Am. Chem. Soc.* **2010**, *132*, 3270.
(37) Williams, G.; Seger, B.; Kamat, P. V. *ACS Nano* **2008**, *2*, 1487.
(38) Wyckoff, R. W. G. *Crystal Structures*; Krieger: Malabar, FL, 1986.
(39) Koma, A. *Thin Solid Films* **1992**, *216*, 72.
(40) Koma, A. *J. Cryst. Growth* **1999**, *201*, 236.
(41) Parkinson, B. A.; Ohuchi, F. S.; Ueno, K.; Koma, A. *Appl. Phys. Lett.* **1991**, *58*, 472.
(42) Meister, S.; Peng, H. L.; McIlwrath, K.; Jarausch, K.; Zhang, X. F.; Cui, Y. *Nano Lett.* **2006**, *6*, 1514.
(43) Peng, H. L.; Meister, S.; Chan, C. K.; Zhang, X. F.; Cui, Y. *Nano Lett.* **2007**, *7*, 199.
(44) Peng, H. L.; Schoen, D. T.; Meister, S.; Zhang, X. F.; Cui, Y. *J. Am. Chem. Soc.* **2007**, *129*, 34.
(45) Peng, H. L.; Zhang, X. F.; Twesten, R. D.; Cui, Y. *Nano Res.* **2009**, *2*, 327.
(46) Richter, W.; Becker, C. R. *Phys. Status Solidi B* **1977**, *84*, 619.
(47) Ferrari, A. C.; Meyer, J. C.; Scardaci, V.; Casiraghi, C.; Lazzeri, M.; Mauri, F.; Piscanec, S.; Jiang, D.; Novoselov, K. S.; Roth, S.; Geim, A. K. *Phys. Rev. Lett.* **2006**, *97*, 187401.

DOI: 10.1021/nl100938e | *Nano Lett.* **2010,** *10,* 2870–2876

(48) Dresselhaus, M. S.; Jorio, A.; Hofmann, M.; Dresselhaus, G.; Saito, R. *Nano Lett.* **2010**, *10*, 751.
(49) Shahil, K. M. F.; Hossain, M. Z.; Teweldebrhan, D.; Balandin, A. A. *Appl. Phys. Lett.* **2010**, *96*, 153103.
(50) Yuzyuk, Y. I.; Katiyar, R. S.; Alyoshin, V. A.; Zakharchenko, I. N.; Markov, D. A.; Sviridov, E. V. *Phys. Rev. B* **2003**, *68*, 104104.
(51) Dobal, P.; Bhaskar, S.; Majumder, S.; Katiyar, R. *J. Appl. Phys.* **1999**, *86*, 828.
(52) Wedler, G.; Schneider, C. M.; Trampert, A.; Koch, R. *Phys. Rev. Lett.* **2004**, *93*, 236101.
(53) Fillon, A.; Abadias, G.; Michel, A.; Jaouen, C.; Villechaise, P. *Phys. Rev. Lett.* **2010**, *104*, 096101.
(54) Springholz, G.; Wiesauer, K. *Phys. Rev. Lett.* **2001**, *88*, No. 015507.
(55) Montazeri, M.; Fickenscher, M.; Smith, L. M.; Jackson, H. E.; Yarrison-Rice, J.; Kang, J. H.; Gao, Q.; Tan, H. H.; Jagadish, C.; Guo, Y.; Zou, J.; Pistol, M.-E.; Pryor, C. E. *Nano Lett.* **2010**, *10*, 880.
(56) Mohiuddin, T. M. G.; Lombardo, A.; Nair, R. R.; Bonetti, A.; Savini, G.; Jalil, R.; Bonini, N.; Basko, D. M.; Galiotis, C.; Marzari, N.; Novoselov, K. S.; Geim, A. K.; Ferrari, A. C. *Phys. Rev. B* **2009**, *79*, 205433.
(57) Huang, M.; Yan, H.; Chen, C.; Song, D.; Heinz, T.; Hone, J. *Proc. Natl. Acad. Sci. U.S.A.* **2009**, *106*, 7304.
(58) Shivaraman, S.; Barton, R. A.; Yu, X.; Alden, J.; Herman, L.; Chandrashekhar, M. V. S.; Park, J.; McEuen, P. L.; Parpia, J. M.; Craighead, H. G.; Spencer, M. G. *Nano Lett.* **2009**, *9*, 3100.
(59) Metzger, C.; Rémi, S.; Liu, M.; Kusminskiy, S. V.; Castro Neto, A. H.; Swan, A. K.; Goldberg, B. B. *Nano Lett.* **2010**, *10*, 6.

DOI: 10.1021/nl100938e | *Nano Lett.* **2010,** *10,* 2870--2876